BULLETIN OF THE POLISH ACADEMY OF SCIENCES
TECHNICAL SCIENCES, Vol. 73(5), 2025, Article number: e154721
DOI: 10.24425/bpasts.2025.154721

Influence of rivet material and squeeze force on the riveting process and residual stresses in riveted joints used in aircraft structures

Adam KORBEL, Valeria MANITCAIA*, and Tomasz MACHNIEWICZ

AGH University of Krakow, Faculty of Mechanical Engineering and Robotics, al. A. Mickiewicza 30, 30-05 Krakow, Poland

Abstract. The paper presents the results of experimental research and finite element analyses (FEA) on the impact of the aircraft rivet installation process and the type of rivet material on the geometric parameters of the driven rivet head, rivet hole expansion (relative interference), residual stresses in sheets, clamping stress and clamping force between sheets in three-row riveted lap joints, as well as linking the obtained results with observations of fatigue crack initiation sites in real riveted joints. The research was conducted for universal head rivets (MS20470AD5-5 and MS20615-5M5) with a shank diameter of 3.96 mm and a length of 7.94 mm, made of two materials, namely aluminium alloy (2117-T4) and nickel-copper alloy (Monel 400), used to join two AA2024-T3 sheets with a thickness of 1.0 mm and 1.6 mm. The experimental tests focused on determining the mechanical properties of sheet and rivet materials (using the digital image correlation DIC technique), geometric parameters of driven rivet heads, and rivet hole expansion, depending on the rivet material and the riveting force level. The results obtained from the numerical models revealed that at the same degree of rivet squeezing, rivets made of Monel 400 generate significantly higher negative residual stresses and residual clamping than rivets made of AA2117-T4, which will affect the contribution of friction to load transfer by a given rivet row and the fretting phenomenon in real riveted joints. The region of compressive residual hoop stress in sheets and the clamping force influence the fatigue crack initiation site and the crack path.

Keywords: riveting process; rivet material; finite element analysis (FEA); residual stress; fatigue crack initiation site.

1. INTRODUCTION

The invaluable advantages of riveted joints [1–4] make them still extensively utilized in aerospace structures for joining thin sheets of helicopter and aircraft fuselages, and other elements stiffening these structures, such as frames or stringers [5–7]. Simultaneously, these joints remain fatigue-critical areas of the aerospace structures, as evidenced by reports and documents of the National Transportation Safety Board (NTSB) and the Federal Aviation Administration (FAA), revealing the presence of numerous fatigue cracks in riveted joints of many airplanes and helicopters [8–11], and the so-called – multiple site damage (MSD) phenomenon [6, 12]. The fatigue life prediction methods for riveted lap joints used in aerospace [13–15], despite their gradual evolution [16–19], are most often semi-empirical methods, based on the results of multidirectional experimental studies. For this reason, they require precise quantification of all phenomena occurring during the element joining process and their cyclic (fatigue) loading.

Riveted joints belong to the group of connections, in contrast to bolted joints, in which the plastic deformation process of the fastener during its installation causes permanent deformations around the rivet hole and residual stresses in the joined elements. The residual deformations occurring in the joint, which result in the rivet hole expansion, and the residual stresses around the rivet hole, as well as the clamping force of the joined elements during external cyclic loading have a fundamental impact on the fatigue crack nucleation location [20–23], the crack path [16, 24, 25], the fretting phenomenon [8, 26, 27] and the fatigue life of the entire structure [28–31]. Figure 1 presents in a simplified way the complex influence of many different and interconnected design and technological factors, and materials of joint elements on various phenomena (often interrelated) occurring in riveted lap joints, affecting their fatigue properties. The research results indicate that even with a selected geometric configuration of rivets and sheets, joint materials, and rivet configuration in a riveted joint, a rise in the squeeze force (F_{sq}) level (before joint loading) increases the residual clamping between the joined elements (clamping stresses σ_{CL} and clamping force P_{CL}) [8, 28, 32, 33] and causes a larger rivet hole expansion [34–37], also known as relative interference (*he*). Higher residual clamping leads to both a greater friction force (T_{FR}) between the joined sheets [8, 26, 38] and a larger stiffening area beneath the rivet heads, which affects the secondary bending phenomenon [39–41] during the loading of the lap joint. The increase in rivet hole expansion changes the value of the residual stresses around the rivet hole and often also their nature (from tensile to compressive) [8, 42–44], and influences the load transfer (transfer force T_{TR}) through subsequent rivet rows during joint loading [45–47]. The joint element materials and each of the design and technological factors presented in Fig. 1 cause a disproportionate quantitative change through

*e-mail: valman@agh.edu.pl

Manuscript submitted 2025-02-13, revised 2025-04-28, initially accepted for publication 2025-05-11, published in August 2025.

the squeeze force in the above-mentioned (and interacting) parameters generated by the riveting process and the joint load level, consequently changing the load transfer method and the crack formation mechanisms, and thus the fatigue life (N_f) of the riveted joint.

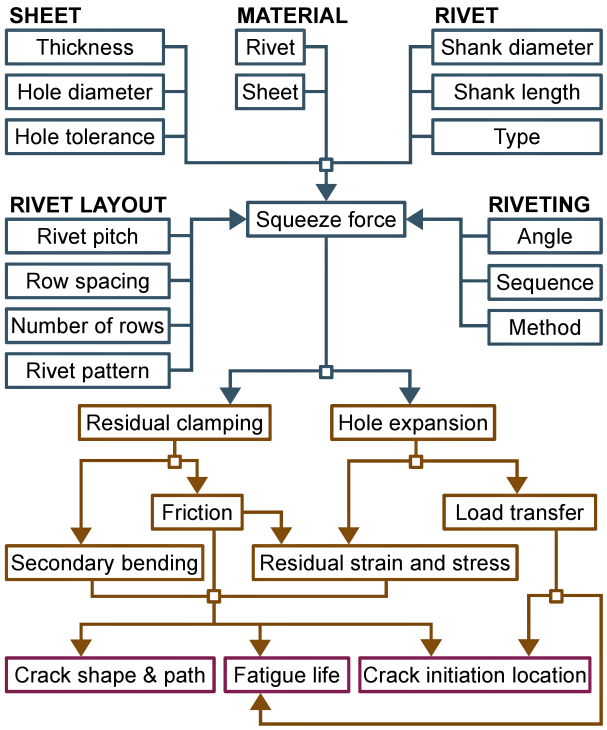

Fig. 1. Factors influencing the fatigue response of a riveted lap joint

The consideration presented above shows that the study of the influence of respective production variables of riveted joints and precise quantification of all parameters related to the riveting process that affect the fatigue life of riveted joints is not a simple process. Apart from difficult, time-consuming and expensive experimental tests, the finite element method (FEM) has become a very convenient and extremely useful tool for extensive research on riveted joints. Finite element (FE) models and finite element analyses (FEA) enable the study and quantification of many phenomena and parameters that are sometimes not easy or even impossible to determine experimentally. However, a word of caution is needed because an improperly developed numerical model and incorrect assumptions made during its definition, and even more so the lack of its validation, may lead to completely erroneous results and conclusions. In the literature on riveted joints, it can be observed that works presenting the results of the FE analyses of the riveting process often do not contain any information on the validation of the developed FE model, or are limited only to the inspection of primary parameters, such as the dimensions of the rivet driven head. Moreover, the parameters of the material models used in these works in the FE models often do not come from authors' own experimental tests, but from works found in the literature, which may vary considerably for a given material depending on the material provided [8, 48]. There is also little research work on the distribution of residual clamping stress and the magnitude of the clamping force generated between the thin sheets in the joints with aluminium aircraft rivets after the riveting process, which significantly affects the value of load transfer through the critical rivet rows and the fretting phenomenon and, consequently, the fatigue behaviour of the riveted lap joints. There is also a lack of information in the literature on the mechanical properties of aircraft rivets made of a nickel-copper alloy (Monel 400), as well as research on joints made with this type of rivets.

The paper presents the research results of the mechanical properties of sheet and rivet materials typically used in aircraft structures and the experimental test results of the installation process of the investigated rivets at different squeeze force levels. A three-dimensional finite element model of the riveting process and the results of numerical analyses related to the influence of the considered variables on the residual stresses in the investigated riveted joints are also presented. The FE model was validated by comparing the numerically predicted and experimentally determined driven rivet head shapes, driven rivet head diameters, and driven rivet head heights, as well as the distribution and magnitude of rivet hole expansion. The performed experimental tests included study of the effect of the rivet material and the degree of rivet squeezing on the geometric parameters of the driven rivet head (primary indicators of the riveting process quality in the aerospace industry) and the expansion of the rivet hole. The numerical analyses focused on the study of the influence of the riveting process and the mechanical properties of the rivets on the distribution and the value of residual stresses in the sheets, the distribution and the range of residual clamping stress on the faying surface of the sheets, and the magnitude of clamping force between the sheets. Based on the current authors' knowledge, there appears to be no research on Monel 400 material used for MS20615 rivets, as well as experimental and numerical investigations on joints with rivets made of Monel 400 in the literature or comparison with MS20470 rivets made of AA2117-T4.

2. MECHANICAL PROPERTIES OF SHEETS AND RIVETS

The research considered riveted joints composed of aircraft aluminium alloy sheets (AA2024-T3 Alclad) with two different thicknesses (t) of 1.0 mm and 1.6 mm and rivets with a diameter (d) of 3.96 mm made of two different materials, i.e., aluminium alloy (AA2117-T4) and nickel-copper alloy (Monel 400). As previously stated, depending on the material supplier the mechanical properties of a specific material may vary significantly. Static tension (sheet material) and compression (rivet material) tests were conducted to determine the precise material properties of the elements of the examined riveted joints, which are essential for the accurate definition of material models within the elastic and plastic range in the FE models.

2.1. Geometry of specimens

For static tensile tests of sheet material (AA2024-T3), with thicknesses of 1.0 mm and 1.6 mm, four flat specimens were used for each sheet thickness, compliant with ISO 6892-1:2009 standard [49], with the geometry shown in Fig. 2a. The speci-

mens were cut out from the same sheet as the elements of the riveted joint using high-pressure water jet cutting technology. Each specimen was oriented such that its axial loading direction was perpendicular to the rolling direction of the sheet. This is consistent with the most common orientation of the skin sheets in a pressurized fuselage, considering that the axial loading on the specimens represents the circumferential stress [50]. In the case of static compression tests of rivet materials (AA2117-T4 and Monel 400), solid cylindrical specimens with a diameter of 3.96 mm and a length of 5.4 mm were used (Fig. 2b). The ratio of both dimensions, according to the ASTM E9 standard [51], classifies them as short specimens. The selected length and diameter of the specimens resulted from the fact that these specimens were cut out from rivets used in riveted joint tests. The specimens were fabricated on a lathe by removing the manufactured rivet head and the rivet shank end.

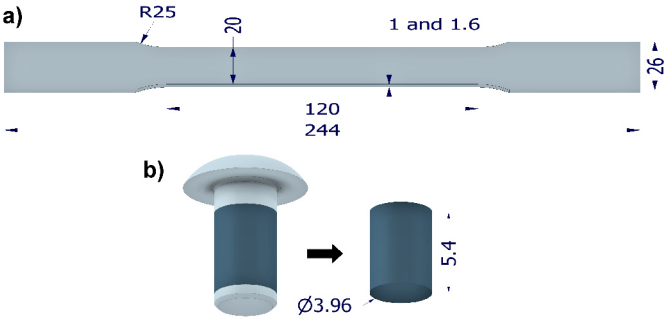

Fig. 2. Geometry and dimensions (mm) of specimens used in: (a) tensile test of sheet material; (b) compression test of rivet material

2.2. Test stand and test parameters

Tension and compression tests were performed on an MTS 810 servo-hydraulic test machine controlled by an MTS FlexTest SE controller and TestWorks 4 software. Static tensile tests of the sheet material were carried out in accordance with the PN-EN 10002-1:2004 standard [52], where strains in the longitudinal direction of the specimen were measured using an Epsilon 3542-025M-025-ST extensometer with a gauge length of 25 mm and a measuring range of ±6.25 mm, and in the transverse direction using an Epsilon 3575-250M-ST extensometer with adjustable gauge length and a measuring range of ±2.5 mm (Fig. 3a). During the tensile test, in the elastic range the stress rate (σ') was close to 10 MPa·s^{-1}, while in the plastic range the strain rate (ε') was close to 0.0012 s^{-1}. Static compression tests were conducted under conditions similar to those specified in the ASTM E9 standard, and strain measurements were conducted using the digital image correlation (DIC) technique. For this purpose, a Dantec Dynamics Q-400 measurement system equipped with two 5.0 Mpx cameras and an LED illumination system was used, as shown in Fig. 3b. The analysis of the strain fields recorded by the DIC Q-400 system for the tested specimens was performed using Istra 4D software, which enables evaluation and visualization of the recorded measurement results [53]. Compression tests were performed at a test speed of 0.162 mm/min, which corresponds to a strain rate (ε') of 0.0005 s^{-1}.

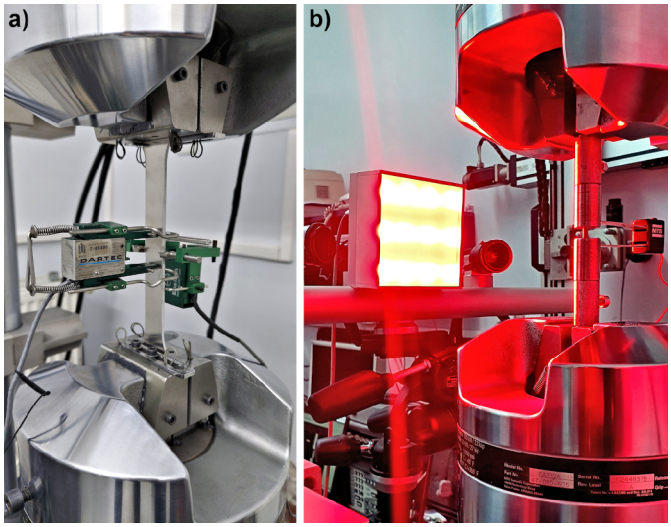

Fig. 3. Testing equipment for static tests: (a) tensile test of sheet material with two contact extensometers; (b) compression test of rivet material using a Dantec Dynamics Q-400 DIC system

2.3. Tension and compression test results

Figure 4a shows representative engineering and true (for the plastic range) stress-strain curves of the analyzed sheet mate-

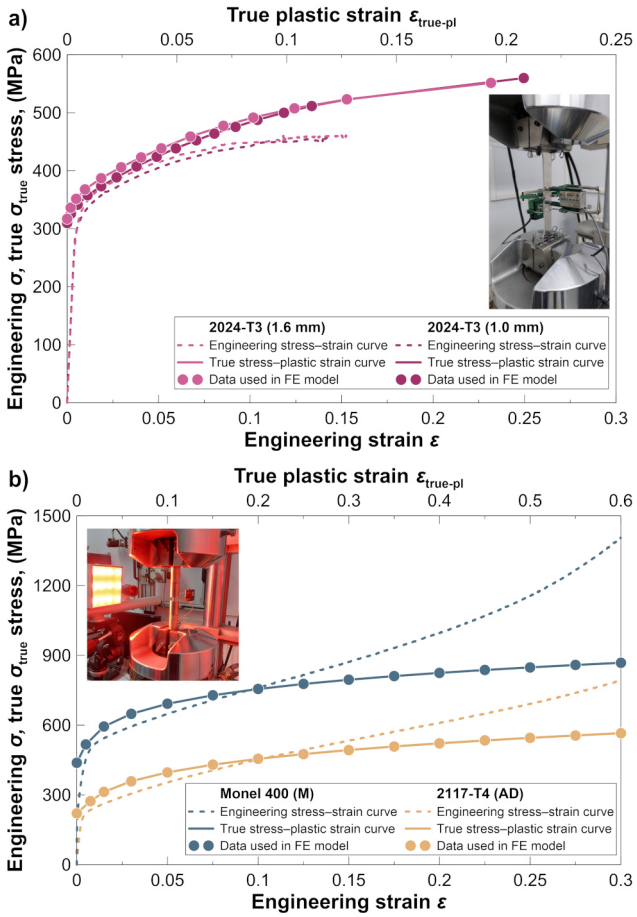

Fig. 4. Engineering σ–ε and true σ_{true}–$\varepsilon_{true-pl}$ curves obtained from tensile and compression tests and the values used in the FE model: (a) sheet material (1.0 mm and 1.6 mm); (b) rivet material (AA2117-T4 and Monel 400)

rial, determined from the tensile tests. The results indicate that the engineering (σ–ε) and true (σ_{true}–$\varepsilon_{\text{true-pl}}$) curves for both considered sheet thicknesses (1.0 mm and 1.6 mm) nearly coincide. The obtained average values of Young's modulus (E = 70 GPa for both sheet thicknesses), Poisson's ratio (ν = 0.33 for both sheet thicknesses) and yield strength ($S_{0.2}$ = 310 MPa for 1.0 mm and $S_{0.2}$ = 317 MPa for 1.6 mm) are typical for the investigated 2024-T3 aluminium alloy and are consistent with literature results [54,55], at the same time exceeding the required minimum values specified by MIL-HDBK-5H [56].

Representative engineering σ–ε and true σ_{true}–$\varepsilon_{\text{true-pl}}$ curves obtained from compression test for rivets material made of AA2117-T4 and Monel 400 are presented in Fig. 4b. Research shows that despite the comparable Poisson's ratio values for both rivet materials (ν = 0.33 for AA2117-T4 and ν = 0.32 for Monel 400), Young's modulus value of the rivet material made of the Monel 400 is almost 2.5 times higher (E = 173 GPa) than the rivet material made of the AA2117-T4 (E = 70 GPa). Similarly, rivets made of Monel 400 have twice the yield strength (438 MPa) than rivets made of AA2117-T4 (221 MPa).

3. EXPERIMENTAL RESEARCH OF RIVETING PROCESS

3.1. Geometry of riveted joints and riveting process

The research was conducted on riveted joints made of rivets and sheets used in the aircraft industry. The study included two types of riveted joints, where one type of joint used universal head MS20470AD5-5 [57] rivets made of 2117-T4 aluminium alloy (AD rivets), while the second type used MS20615-5M5 [58] rivets made of Monel 400 nickel-copper alloy (M rivets). Both types of rivets had nominal shank diameter of d = 3.96 mm and shank length of l = 7.94 mm, and their geometry and dimensions are shown in Fig. 5. Each riveted joint composed of two 2024-T3 Alclad aluminium alloy sheets of different thicknesses (t = 1.0 mm and t = 1.6 mm).

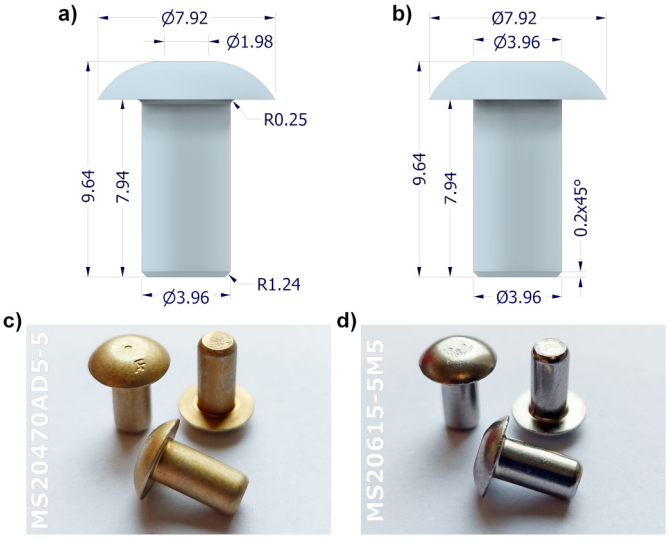

Fig. 5. Geometry and dimensions (mm) of universal head rivets: (a) used in the experimental tests; (b) adopted in the FE model; (c) MS20470-AD5-5; (d) MS20615-5M5

2×10 specimens were used for the investigation of the influence of the squeeze force (F_{sq}) and the rivet material on the diameter (D) and height (H) of the driven rivet head, as well as on the rivet hole expansion (he), with the geometry and dimensions shown in Fig. 6. These specimens were cut from the same sheets as the tensile test specimens using high-pressure water jet cutting technology. The sharp edges left after the water-cutting process were removed using a deburring machine. After the two sheets forming the joint were pressed together, rivet holes were drilled at one fastening using a drill with a nominal diameter of d_{d} = 4.07 mm. Then the edges of the rivet holes on both sides of the sheet were deburred ($0.1 \times 45°$). This operation is also used in the aircraft industry for the removal of sharp edges and burrs created after the hole-drilling process.

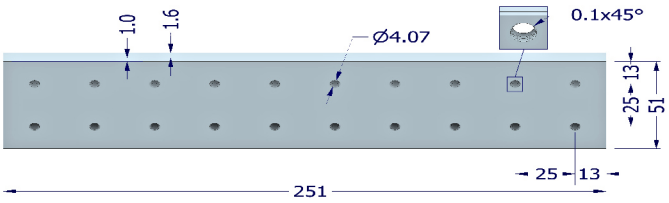

Fig. 6. Geometry and dimensions (mm) of specimens for experimental research on the riveting process

Riveting of investigated joints was performed in a static way with a controlled force on the MTS 810 testing machine. The riveting process was conducted at a punch speed of v_{p} = 25 mm/min until the assumed F_{sq} force was achieved. A special riveting tool (squeezer) shown and described in [31] was used during the installation of the rivets in the specimens. This tool ensured the preliminary clamping of the jointed sheets and the proper alignment of the rivet with both the punch and the rivet hole. It also guaranteed the formation of an axially symmetrical driven rivet head during the riveting process. The rivets were installed in the specimens in such a way that the manufactured rivet head was on the side of the thinner sheet (t = 1.0 mm).

3.2. Effect of squeeze force and rivet material on the driven rivet head dimensions

The D/d ratio in the aircraft industry, which is the ratio of the driven rivet head diameter (D) and the rivet shank diameter (d), is usually considered as a first and basic quality control criterion for riveted joints [6, 8]. This is due to the fact that for a given rivet type, joint geometry, and joint materials, the D/d ratio is closely related to the F_{sq} force. In general, it can be stated that depending on the combination of selected rivets and sheets, the application of the joint, and the manufacturer of the aviation industry, the commonly accepted values of the D/d ratio are in the range of 1.25÷1.8 [8, 28, 59, 60]. The second indicator of the quality of the riveting process is the H/h ratio, which is the ratio of the driven rivet head height (H) and the initial height of the rivet shank above the surface of the joined sheets (h).

After installation of rivets in specimens with different F_{sq} forces, the driven rivet head diameters (D) were measured using a calliper with an accuracy of 0.01 mm in two mutually

perpendicular directions, and based on this the average value of the driven rivet head diameter was determined for a given F_{sq} force and a given rivet material. Then, the heights of the driven rivet heads (H) were measured with an accuracy of 0.01 mm using an electronic dial gauge, by measuring the offset of the tip of the dial gauge located in the centre of the driven rivet head relative to the sheet surface.

Figure 7 presents the influence of the squeeze force (F_{sq}) and the rivet material (AA2117-T4 and Monel 400) on the normalized driven rivet head dimensions (D/d and H/h) for the considered joints, determined from experimental measurements. As expected, an increase in the F_{sq} force causes a systematic increase in the D/d ratio and an opposite trend in the H/h ratio regardless of the rivet material. As can be seen, in the entire analyzed range of D/d and H/h ratios, rivets made of Monel 400 require a definitely higher F_{sq} force (42%÷55%) to obtain the same D/d and H/h ratio than rivets made of the AA2117-T4. For example, to obtain the most commonly used ratio $D/d = 1.5$ AD rivets require a force of $F_{sq} = 15.5$ kN, while M rivets require a force of $F_{sq} = 22.9$ kN, which is almost 1.5 times greater.

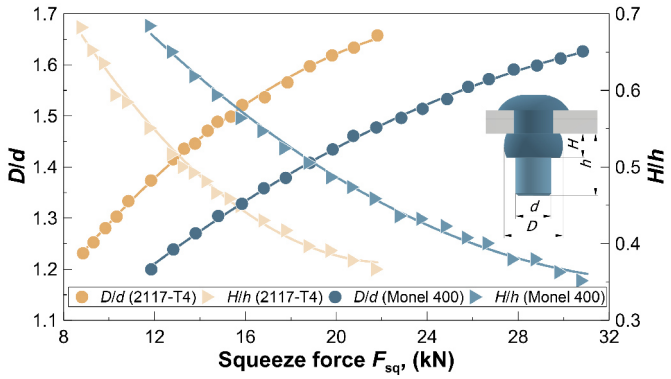

Fig. 7. Effect of the F_{sq} force on the D/d and H/h ratios obtained from experimental measurements for rivets made of AA2117-T4 and Monel 400

The relationships between the D/d and H/h ratios and the F_{sq} forces determined in this section will be used later to validate the developed FE models in the entire range of the analyzed F_{sq} forces. Then, the determined values of the F_{sq} forces for a given rivet material will be used as input data for the FE models utilized for residual stresses analysis in the studied riveted joints. Furthermore, the obtained values of the F_{sq} forces for each rivet material, corresponding to the ratios $D/d = 1.3$, $D/d = 1.5$ and $D/d = 1.6$, will be used in the next part of the experiments to carry out measurements related to the rivet hole expansion (he).

3.3. Rivet hole expansion measurements

The rivet hole expansion (he) is a crucial and experimentally measurable parameter related to the riveting process, which has a direct impact on the residual stresses in the joined sheets. This parameter is defined as $he = (d_e - d_0)/d_0$, where d_0 and d_e are the rivet hole diameters before and after riveting, respectively.

Rivet hole expansion measurements were performed using the previously developed measurement method [29]. The first step in this method involves removing the manufactured and driven rivet heads located above the surfaces of the connected sheets. In the second step, the specimen surface is milled in a plane perpendicular to the rivet axis to the desired z_1 depth. In the third step, the milled specimen surface is ground and then polished (and etched, if necessary) to facilitate observation of the boundary between the rivet and the sheet. In the fourth step, the rivet hole diameter (d_e) is measured under a microscope. After measuring he, the specimen is milled to subsequent z_i depths at which the next diameters (d_{ei}) are measured. The rivet hole expansion measurements can be performed simultaneously on both sides of the joint.

The same manner and the same riveting tool as described in Section 3.1 were applied for the riveting of the specimens used to investigate the effect of the F_{sq} force and the rivet material on he. The hole expansion was measured for thinner sheets ($t = 1.0$ mm) at a depth of $z_1 = 0.5$ mm, while for thicker sheets ($t = 1.6$ mm) it was assessed at a depth of $z_1 = 0.2$ mm and then $z_2 = 0.8$ mm. Milling of the specimens to the appropriate z_i depth (including removal of the rivet heads) was performed on a Haas Mini Mill CNC milling machine. Measurements of d_0 and d_e individually for each rivet hole were performed in two mutually perpendicular directions using a Keyence VHX-600 digital microscope at a magnification of 50x and with a measurement accuracy of 10^{-3} mm.

Figure 8 shows the average values of he achieved from three samples during the experimental measurements for the considered rivet materials and different degrees of rivet squeezing (D/d). The results indicate that, regardless of the rivet material and the measurement location, he systematically increases with the increase of the F_{sq} force. It can be seen that for each of the analyzed rivet materials (AA2117-T4 and Monel 400) the value of he in the sheet next to the manufactured head is significantly smaller than in the sheet next to the driven rivet head. This can be explained by the fact that during the riveting process, the plastic deformations of the rivet in the radial direction are significantly larger on the driven head side than on the manufactured head side. The manufactured head is integrated with the rivet shank, which makes it difficult to freely deform the shank in this place towards the rivet hole, while the other side of the rivet, where the driven rivet head is formed, deforms much more easily under the action of the riveting punch, and the only resistance that

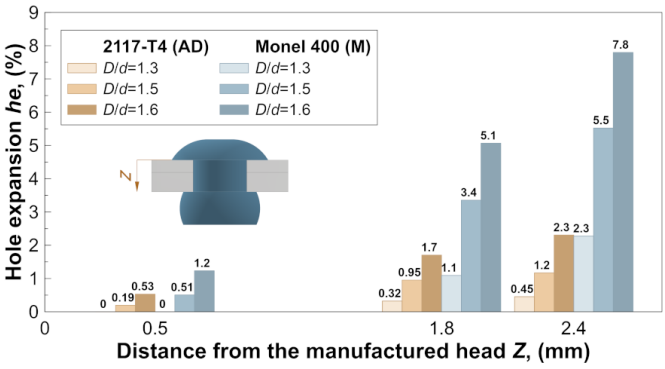

Fig. 8. Average values of he obtained from measurements for two rivet materials (AA2117-T4 and Monel 400) and D/d ratio of 1.3, 1.5 and 1.6

occurs in this place is the friction force between the rivet (driven rivet head) and the riveting tool. The analysis of the effect of the rivet material on *he* proves that regardless of the value of the D/d ratio, both on the side of the driven rivet head and on the side of the manufactured head, the hole expansion for M rivets is much larger (2.2÷5.1 times) than for AD rivets. This indicates that a rivet made of a harder nickel-copper alloy (Monel 400) deforms the sheet material (AA2024-T3) around the rivet hole much more easily than a rivet made of a softer aluminium alloy (2117-T4). It should be noted that the percentage difference in *he* between the considered rivet materials decreases with an increase in the D/d ratio.

4. FE MODEL DESCRIPTION

Numerical analyses were conducted utilizing the ANSYS Mechanical 2021 R2 environment [61]. Due to the complexity of the analyzed issue, the developed three-dimensional (3D) FE models took into account the non-linear material behaviour of the rivets and sheets, the contact and friction conditions between all cooperating elements (both the joint elements and the riveting tools), and the boundary non-linearity resulting from the varying contact conditions between the surfaces of the sheets and the rivet. To consider the mutual interaction of adjacent rivets in the joint, FEA was performed for three-row riveted lap joints, which are a typical type of connection for longitudinal joints of the aircraft fuselage [8, 59]. Given the constant pitch of the rivet in each row (p = 20 mm), the FE analyses were performed for a representative joint fragment with a length of 226 mm and a width of 20 mm, with one rivet in each row, as shown in Fig. 9. The analyzed joint, as in the case of experimental tests, consisted of two aluminium sheets with a thickness of 1.0 mm and 1.6 mm and universal head MS20470AD5-5 and MS20615-5M5 rivets. To precisely reproduce the real geometry of the analyzed riveted joints, the chamfering of the rivet hole edges (0.1×45°) was also included in the FE models (see Section 3.1). In order to obtain high regularity and better quality of mesh in the FE models, slight simplifications were introduced in the geometry of the used rivets, as shown in Fig. 5b. It was assumed, namely, that the diameter of the flat upper surface of the manufactured rivet head is the same as the diameter of the rivet shank (Ø3.96 mm). Furthermore, the rounding with a radius of R0.25 mm under the manufactured rivet head was removed, and the radius of R1.25 mm at the end of the rivet shank was replaced with a 0.2 mm×45° chamfer.

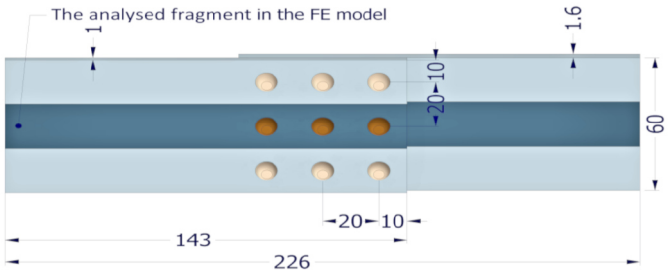

Fig. 9. Geometry and dimensions (mm) of riveted lap joints adopted in the FE models

4.1. Material models for rivets and sheets

The sheets and rivets in the FE models were modelled as flexible bodies defined by elastic-plastic material models with multilinear isotropic hardening, used in the analyses of large plastic deformations. The riveting tools (hold-ons and punches) were modelled as rigid bodies. The material models of sheets (AA2024-T3) and rivets (AA2117-T4 and Monel 400) were defined based on the experimental tests described earlier (see Section 2.3). The elastic range was specified based on experimentally determined values of Young's modulus (E) and Poisson's ratio (ν). The curves in the plastic range were defined in a discrete form by providing data for points located on the experimentally determined σ_{true}–$\varepsilon_{\text{true-pl}}$ curves shown in Fig. 4.

4.2. Boundary conditions, loads, and FE model parameters

The boundary conditions and the load implementation method adopted in FEA are shown in Fig. 10. Using the symmetry boundary condition concerning the X-Y plane passing through the rivet axes, the calculations were performed for half of the joint, assuming the same behaviour of the elements on the opposite side of the adopted symmetry plane. The second symmetry condition in a plane parallel to the X-Y plane was defined on the edge of the sheets to consider the impact of the remaining part of the joint and the rivets on the analyzed fragment of the riveted joint. All degrees of freedom on the end surfaces of the sheets (outside the overlap) were constrained using the remote displacement option [61], allowing them to move freely only along the X-axis. Similarly, the hold-ons and punches were completely locked using the remote displacement option applied to the side surfaces of these elements, with the difference that the punches could move freely along the rivet axis (Y-axis). The riveting process was conducted in three stages, where in Stage 1 the rivets were compressed and deformed, in Stage 2 the rivets were relieved, and in Stage 3 the riveting sets were moved away. In Stage 1, loads corresponding to squeezing forces (F) were applied to the lower surface of the punches in the Y-axis direction using a remote force option [61], which was gradually increased until the maximum assumed value corresponding to the F_{sq} force was reached. In Stage 2, the F force was slowly decreased to completely relieve the rivets and achieve zero force value on the rivets. In Stage 3, the remote force option was turned off and the remote displacement option in the Y-axis direction applied to the side surfaces of the punches and hold-ons was simultaneously activated so that all riveting tools were moved away from the formed rivet joint.

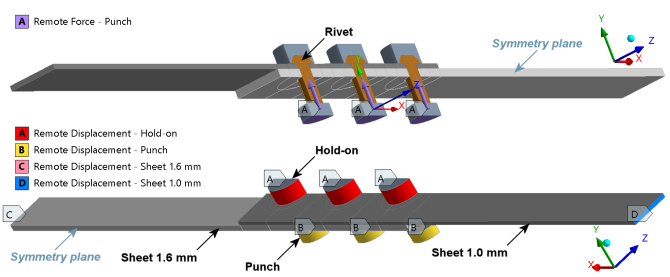

Fig. 10. Boundary conditions and load conditions applied to the solid model in ANSYS software

Due to the strongly non-linear nature of the conducted analyses and the large plastic deformations occurring during the riveting process, Stage 1 of FEA consisted of 30 steps and a large number of sub-steps, Stage 2 comprised three steps, and Stage 3 included two steps. A frictional contact type with a friction coefficient of $\mu = 0.2$ was defined between all mating surfaces [26, 62–64]. To reduce the mutual penetration of bodies, which is of crucial importance in the case of the analyzed issue, and to ensure the highest possible precision of the results, the augmented Lagrange method was used in the contact calculations [65].

4.3. Model discretization

An important stage in the formulation of numerical models is discretization, the quality of which is influenced by the size of the finite elements, their shape, and their arrangement relative to each other. In the developed FE models, all flexible bodies were composed only of higher-order 3D 20-node solid elements (SOLID186), which ensure a shorter calculation time and fill the volume of solids more efficiently than tetrahedral elements [61, 66]. The 8-node quadrilateral and 6-node triangular elements were present only on the surfaces of rigid bodies (punches and hold-ons). Due to the large plastic deformations of the mesh elements occurring during the riveting process, in order to eliminate possible errors in the automatic discretization performed by the ANSYS program, the mesh was modified gradually to obtain the highest possible regularity and the best mesh quality metrics recommended by the software manufacturer [67]. The mesh quality assessment was made based on three metrics, i.e., skewness, orthogonal quality, and Jacobian ratio. Figure 11 shows the FE mesh finally adopted in the developed FE models after modifications. As can be seen, the prepared mesh is denser near the rivet hole and gradually sparse in the radial direction, and the sheets are divided in the thickness direction into eight elements for thicker sheets ($t = 1.6$ mm) and five elements for thinner sheets ($t = 1.0$ mm). With such a mesh selected, the prepared FE models contained 125 821 elements and 567 710 nodes. The analysis of the adopted metrics to evaluate the quality of the prepared mesh showed that all finite elements have at least good skewness (max. 0.61) and orthogonal quality (min. 0.63), and the Jacobian ratio value does not exceed 3.48.

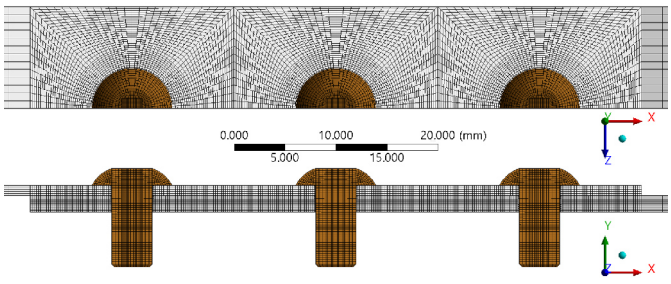

Fig. 11. Mesh adopted in the FE model

5. VALIDATION OF THE NUMERICAL MODEL

The simplest validation of the FE models for the analysis of the riveting process can be performed by a comparison of the driven rivet head dimensions (D and H) obtained from the experiment measurements and FEA. However, it should be noted that achieving the same D and H dimensions does not ensure that the developed FE model correctly predicts the distribution and magnitude of strains and stresses in the joined sheets [8]. Performing the correct validation of the FE model in the case of the riveting process is a challenging and complicated task, because the largest sheet deformations, and thus the greatest stresses generated in the riveted joint at a fatigue-critical location, occur in the areas covered by the manufactured and driven rivet heads. In the current authors' opinion, the most relevant and experimentally measurable parameter that directly affects the residual stresses in the sheets under the rivet heads is the rivet hole expansion. In this paper, the validation of the developed FE models was carried out by comparing the following four parameters obtained from the experimental measurements and numerical analyses: (1) the shape of the driven rivet head, (2) the normalized driven rivet head diameter (D/d), (3) the normalized driven rivet head height (H/h), and (4) the rivet hole expansion (he) at different squeeze forces (F_{sq}).

The preliminary validation of the developed FE models focused on verification of the shape of the driven rivet head after the riveting process, as presented in Fig. 12. As can be seen for both investigated types of rivet (AA2117-T4 and Monel 400) installed with the ratio $D/d = 1.45$, the shape of the driven rivet heads obtained from FEA and observed in experimental tests is barrel-shaped. This initially confirms the correctness of the developed FE model and the carefully selected friction coefficient (μ).

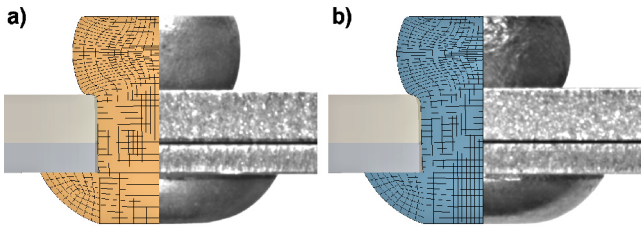

Fig. 12. Comparison of the driven rivet head shape (barrel shape) obtained from the FE model and experimental tests for the D/d ratio of 1.45: (a) MS20470AD5-5 rivets; (b) MS20615-5M5 rivets

In the next step of the validation of the FE models, the normalized driven rivet head dimensions (D/d and H/h) obtained from the experimental tests (see Fig. 7) and FEA were compared for both investigated rivet materials with various values of the F_{sq} forces, as shown in Fig. 13. As can be seen, for both AD and M rivets, the values of the D/d and H/h ratios obtained from the FE analyses are in exceptionally good agreement with the results of the experimental studies. This confirms that the developed FE models correctly predict the deformations of the analyzed rivets during the riveting process and indicates the proper relationship between the F_{sq} force and the characteristic dimensions of the driven rivet head (D and H) in the entire range of the analyzed degrees of rivet squeezing.

In the last step of the validation of the FE models, the values of all experimentally measured hole expansions (see Section 3.3) were compared with the results obtained from numerical analy-

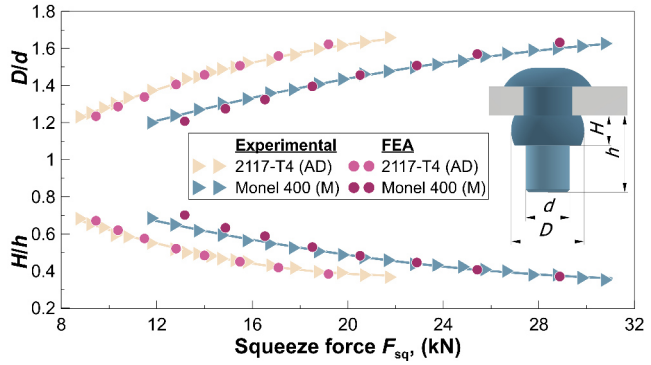

Fig. 13. Comparison of the D/d and H/h ratios as a function of the F_{sq} force obtained from experimental measurements and FE model

ses for both tested rivet materials (AA2117-T4 and Monel 400) at three degrees of squeezing D/d (1.3, 1.5 and 1.6), as shown in Fig. 14. In the case of FEA, the lack of *he* results directly under the rivet heads and on the faying surface of the sheets is related to the chamfering of the edges of the rivet holes (see Fig. 6). As shown, the developed numerical models accurately predict the values and distributions of *he* for all the considered D/d ratios. This proves that the deformations of the rivets and sheets under the manufactured and driven heads were correctly predicted, which again confirms the correctness of the developed FE models. The discrepancies between the results of experimental tests and FEA visible in some places may result from the fact that the *he* measurement is difficult and very sensitive to the measured d_0 and d_e diameters (in two mutually perpendicular directions), which means that a small measurement error of any of these diameters strongly affects the final result of *he*.

The high convergence of four different parameters (the shape of the driven rivet head, D/d, H/h, and *he*) determined from numerical analyses and experimental tests for different F_{sq} forces confirms the validity of the developed FE models for both investigated rivet materials.

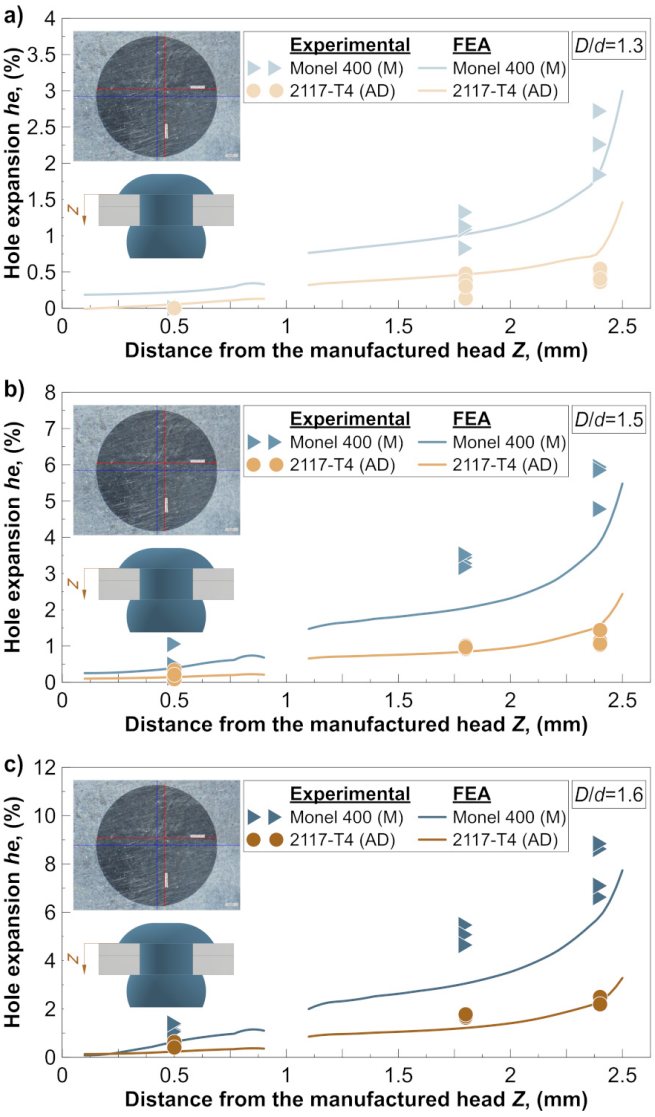

Fig. 14. Comparison of *he* for rivets made of AA2117-T4 and Monel 400 derived from experiments and FEA for D/d ratio: (a) 1.3; (b) 1.5; (c) 1.6

6. RESULTS OF FE ANALYSES AND DISCUSSION

During the riveting process, the rivet deformation causes the expansion of the rivet hole and the clamping of the joined sheets, which generates residual stresses in the formed joint. Evaluation of these stresses was made based on the residual radial (σ_R), hoop (σ_H), and clamping (σ_{CL}) stresses, which can assume positive (tensile) and negative (compressive) values and, as shown in Fig. 1, can influence the fatigue behaviour of riveted lap joints.

6.1. Residual radial stress

Figure 15 shows the distributions of residual radial stresses (σ_R) in the analyzed joints for the two investigated rivet materials (AA2117-T4 and Monel 400) and three D/d ratios (1.3, 1.5, and 1.6) obtained from FEA. As shown, for both investigated rivet materials and all considered D/d ratios, the highest absolute values of the σ_R stresses are observed in the thicker sheet (1.6 mm) in close vicinity to the driven rivet head. This is due to the fact that this location coincides with the location of the highest *he* values (see Fig. 8 and Fig. 14). It is worth noting that the σ_R stress distributions in the sheet thickness direction are also qualitatively consistent with *he* distributions. FEA indicates that for both rivet materials, the σ_R stresses assume negative values almost over the entire thickness of the joined sheets and their value and range increase with the D/d ratio. Additionally, the results obtained from the FE models reveal that for the same degree of rivet squeezing (D/d), the highest negative σ_R stresses are generated in joints with rivets made of Monel 400, and range from 18% (D/d = 1.3) to 43% (D/d = 1.5) higher than the σ_R stresses in joints with rivets made of AA2117-T4. Similarly, the range of these stresses is noticeably larger for M rivets than for AD rivets. This is because the harder Monel 400 rivets with higher mechanical properties ($S_{0.2}$ = 438 MPa) plastically deform the sheet ($S_{0.2}$ = 317 MPa) more easily than the softer AA2117-T4 rivets ($S_{0.2}$ = 221 MPa) (see Section 2.3). Consequently, while riveting a joint with a given geometry at the same

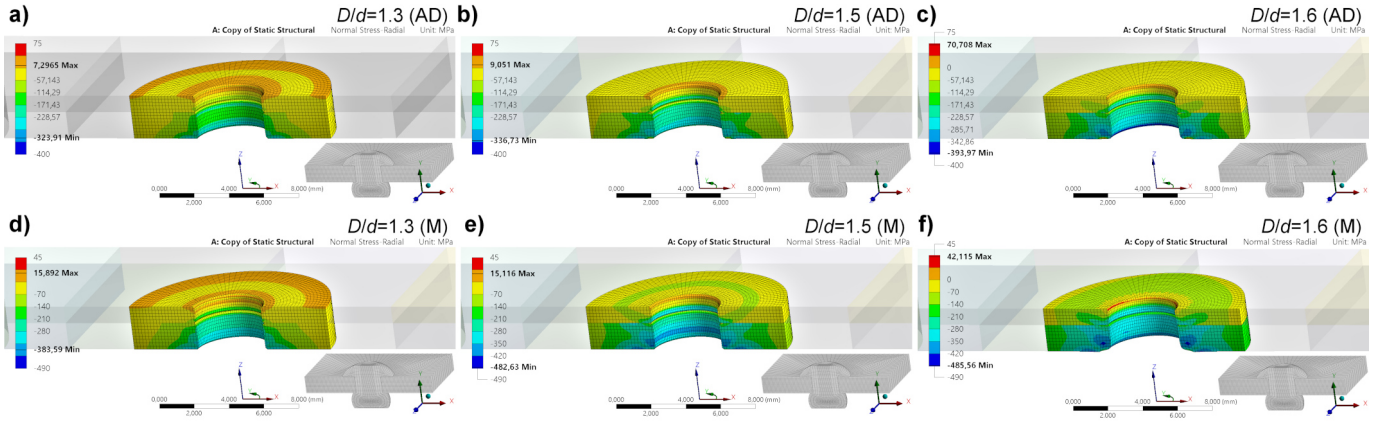

Fig. 15. Distributions of residual radial stresses (σ_R) in sheets for: (a) AD rivets and $D/d = 1.3$; (b) AD rivets and $D/d = 1.5$; (c) AD rivets and $D/d = 1.6$; (d) M rivets and $D/d = 1.3$; (e) M rivets and $D/d = 1.5$; (f) M rivets and $D/d = 1.6$

D/d ratio, the increase in the diameter of the MS20615-5M5 rivet will exceed that of the MS20470AD5-5 rivet, because the sheet material shows less resistance to the expansion of the rivet shank diameter.

6.2. Residual hoop stress

The distributions and values of residual hoop stresses (σ_H) generated in the sheets for the considered rivet materials and D/d ratios are shown in Fig. 16. Regardless of the rivet material, at a small D/d ratio of 1.3, positive (tensile) stresses occur in the sheets around the rivet hole edge in the area of faying surface and under the manufactured rivet head. Increasing the degree of rivet squeezing ($D/d = 1.5$ or $D/d = 1.6$) results in the positive σ_H stresses moving to a certain distance from the rivet hole edge, and negative (compressive) σ_H stresses being generated in its close vicinity. The analysis of the effect of the rivet material on the σ_H stresses generated in the sheets shows that for the same D/d ratio, the zone of negative σ_H stresses is larger and the positive stresses are moved further from the rivet hole in joints with M rivets than in the case of joints with AD rivets. This is an especially important observation because the negative σ_H stresses in the vicinity of the rivet hole reduce the stresses caused by external joint loading [8]. This explains the trend observed by authors in fatigue tests performed for joints with different geometric parameters [17, 18, 68] and friction conditions [26], showing an increase in the fatigue life (N_f) of riveted lap joints with an increase in the D/d ratio.

Fatigue tests indicate that the initiation of fatigue cracks in riveted lap joints occurs on the faying surface of the joined sheets around the rivet hole [8, 21, 26, 27, 29], as shown in Fig. 17 for three-row lap joints of two 1.6 mm thick AA2024-T3 sheets with MS20470AD5-6 rivets at a cyclic stress amplitude (S_a) of 54 MPa and a stress ratio (R) of 0.1. Thus, it is crucial to investigate the residual hoop stresses (σ_H) at this location. Figure 18 shows the distributions of residual σ_H stresses on the faying surface of the sheets (on the sheet side next to the manufactured head and next to the driven head) obtained from FE analyses for the analyzed rivet materials and D/d ratios in the range of 1.25÷1.6. Regardless of the rivet material, small D/d ratios (1.25÷1.3) generate almost entirely positive σ_H stresses in both sheets of the joint (small *he*, see Fig. 8), which reach the highest values of 23÷66 MPa (AD rivets) and 75÷137 MPa (M rivets) at the edge of the rivet hole. An increase in the F_{sq} force changes the nature of these stresses and, starting from the

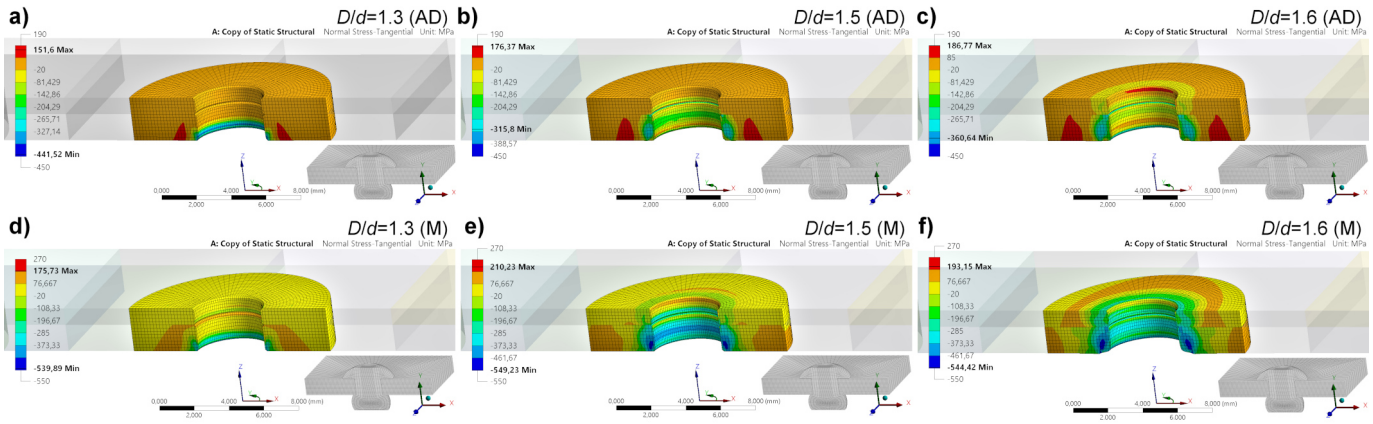

Fig. 16. Distributions of residual hoop stresses (σ_H) in sheets for: (a) AD rivets and $D/d = 1.3$; (b) AD rivets and $D/d = 1.5$; (c) AD rivets and $D/d = 1.6$; (d) M rivets and $D/d = 1.3$; (e) M rivets and $D/d = 1.5$; (f) M rivets and $D/d = 1.6$

ratio $D/d = 1.4$, the positive σ_H stresses are progressively moved away from the rivet hole and, at the same time, increasingly higher favourable compressive stresses are generated around it. It should be pointed out that not only the value but also the range of negative σ_H stresses increases with the increase in the D/d ratio. This explains the effect of the F_{sq} force on the fatigue life and the fatigue crack initiation site in riveted lap joints observed in fatigue tests, where at low F_{sq} forces ($D/d = 1.3$), cracks develop from the edge of the rivet hole (Fig. 17a), whereas at higher F_{sq} forces ($D/d = 1.5$), cracks initiate at a certain distance from the rivet hole (Fig. 17b). Comparison of the results of both rivet materials shows that for a given D/d ratio, rivets made of Monel 400 induce significantly greater σ_H stresses in both joint sheets in terms of value and range than rivets made of AA2117-T4. This is particularly visible at high F_{sq} forces where, for example, for the ratio $D/d = 1.6$ the greatest negative σ_H stresses on the driven head side for M rivets reach values approx. 30% higher than for AD rivets (–301 MPa vs. –392 MPa), while on the manufactured head side this difference increases to approx. 170% (–130 MPa vs. –348 MPa).

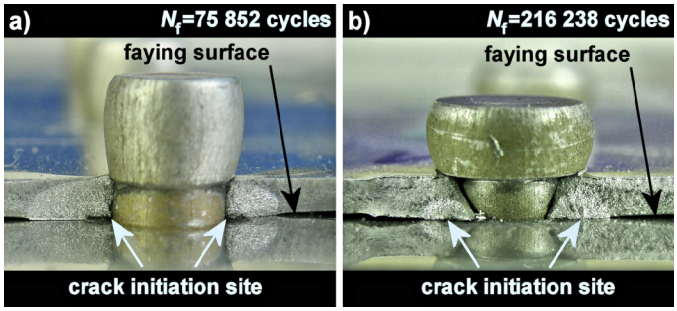

Fig. 17. Influence of the F_{sq} force on the fatigue life (N_f) and the crack initiation site for three-row lap joints of two 1.6 mm thick AA2024-T3 sheets with MS20470AD5-6 rivets: (a) $D/d = 1.3$; (b) $D/d = 1.5$

6.3. Residual clamping stress and clamping force

Once the riveting process is finished, in addition to the hole expansion caused by the deformation of the rivet shank, there is also the effect of pressing the sheets against each other by the rivet heads with an axial force called the clamping force (P_{CL}). This force is non-uniformly distributed around the rivet hole on a relatively small area of the faying surface of the sheets in the form of residual clamping stresses (σ_{CL}). The P_{CL} force during cyclic loading of riveted lap joints affects the percentage of friction force (T_{FR}) in total load transfer (T_{TR}) by individual rivet rows [50,69,70], the fretting phenomenon occurring on the faying surface [8,26,71], and, to some extent, the deflection of the sheets caused by the secondary bending phenomenon [40, 41]. For this reason, it is justified to analyze the effect of the D/d ratio and the rivet material on the value of the P_{CL} force and the distribution and range of the σ_{CL} stress zone.

Figure 19 shows the distributions of the residual clamping stresses σ_{CL} on the faying surface of the sheets obtained from FEA after moving the riveting tools away for both the considered rivet materials (AA2117-T4 and Monel 400) and three D/d ratios (1.3, 1.5 and 1.6), while Fig. 20 presents the detailed

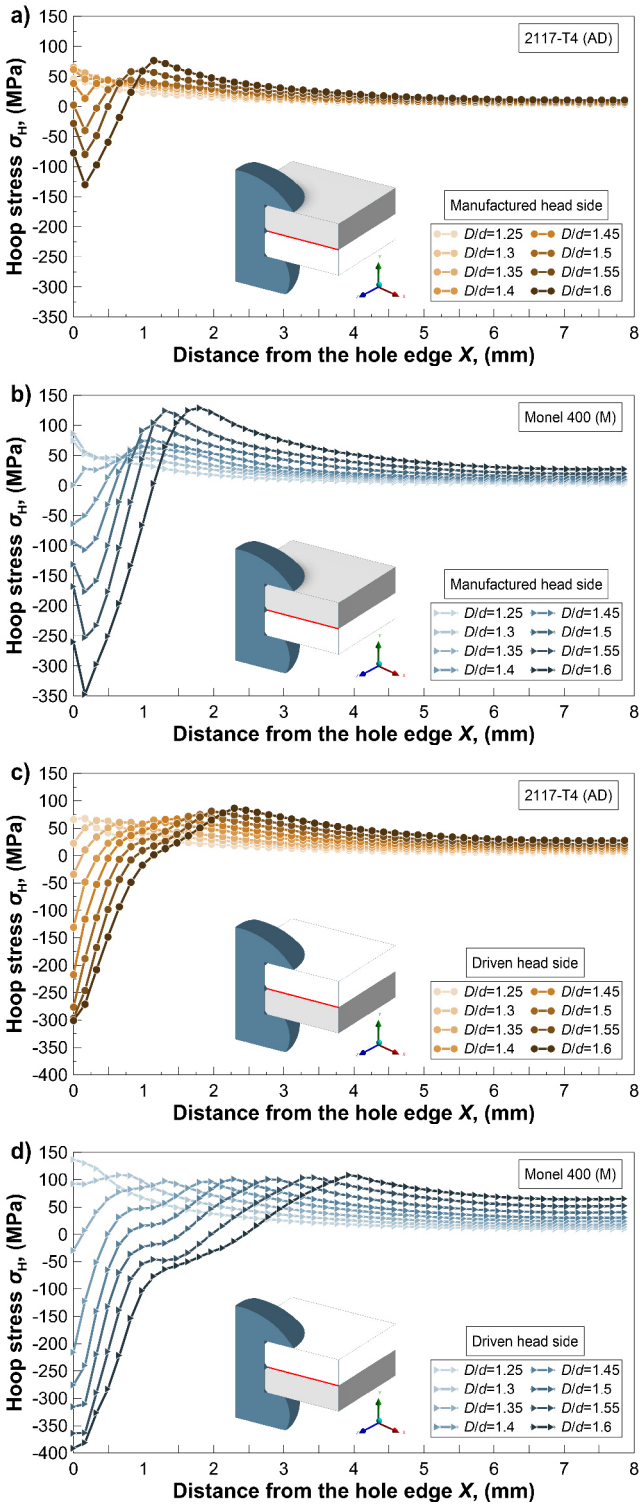

Fig. 18. Effect of the F_{sq} force on residual σ_H stress distribution on the faying surface: (a) AD rivets – manufactured head side; (b) M rivets – manufactured head side; (c) AD rivets – driven head side; (d) M rivets – driven head side

values distribution of these stresses along the path running from the edge of the rivet hole along the Z-axis. FE analyses indicate that, regardless of the applied F_{sq} force and rivet material, the highest values of compressive σ_{CL} stresses are generated at the

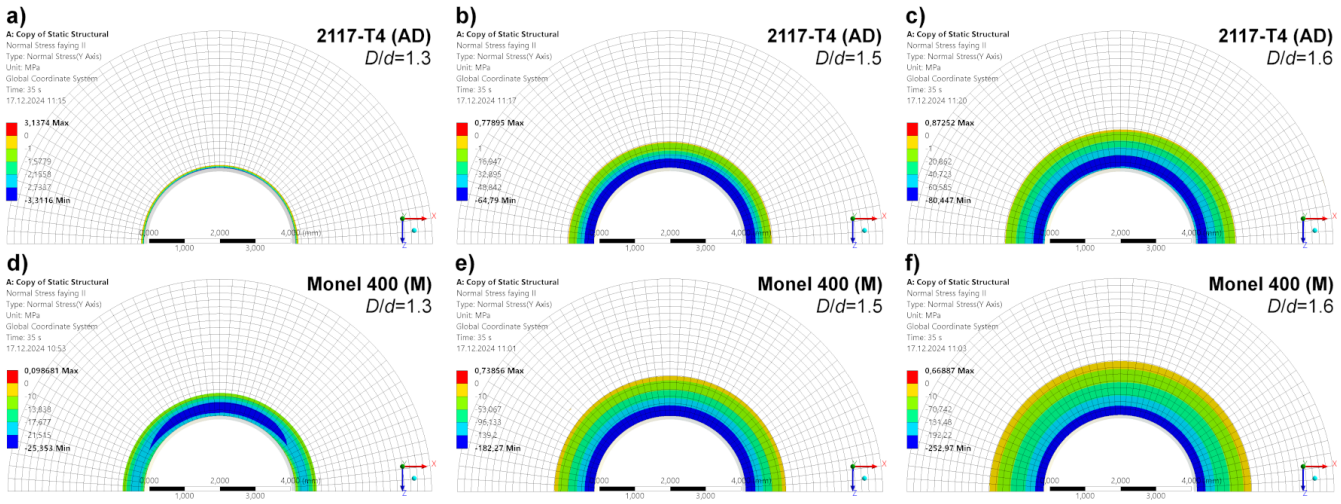

Fig. 19. Distributions of residual clamping stress (σ_{CL}) on the faying surface for: (a) AD rivets and D/d = 1.3; (b) AD rivets and D/d = 1.5; (c) AD rivets and D/d = 1.6; (d) M rivets and D/d = 1.3; (e) M rivets and D/d = 1.5; (f) M rivets and D/d = 1.6

edge of the rivet hole, and their value rapidly decreases with the distance from the rivet hole. Moreover, the increasing D/d ratio is accompanied by systematic growth in the value and range of the residual clamping stress zone. Comparing the effect of the rivet materials, it is evident that at the same D/d ratio, the σ_{CL} stresses in joints with harder rivets (Monel 400) reach several times higher absolute values compared to joints with softer rivets (AA2117-T4). It should be noted that the higher value and the larger annular σ_{CL} stress zone, which occurs at higher D/d ratios and/or M rivets, will cause greater stiffening of the joined sheets under the rivet heads, which to some extent changes the deflection of the lap joint during its loading. This may also affect the distance at which the crack path is shifted from the rivet hole [8]. Furthermore, considering the location of positive σ_H stresses (see Fig. 18), an extensive range of the clamping zone will also contribute to the nucleation of cracks at a distance from the rivet hole.

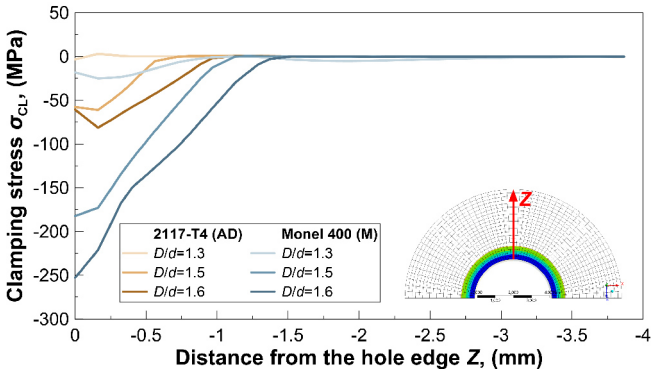

Fig. 20. Effect of the F_{sq} force and rivet material (2117-T4 and Monel 400) on residual clamping stress (σ_{CL}) distribution on the faying surface

The relationship between the clamping force (P_{CL}) and the D/d ratio, the F_{sq} force and the type of rivet material, determined from the FE analyses, is shown in Fig. 21. The P_{CL} force was determined after removing the riveting tools as a reaction force in the direction of the rivet axis (Y-direction) occurring on the contact surface with dimensions of 20 mm × 20 mm (see Fig. 9), i.e., per one rivet. As expected, regardless of the rivet material, the P_{CL} force systematically increases with a growing D/d ratio. At the same time, for the same D/d ratio, the P_{CL} force reaches values significantly higher (3.6÷15.9 times) for joints connected with M rivets than for joints with AD rivets (Fig. 21a). The analysis of the relationship between the F_{sq} force

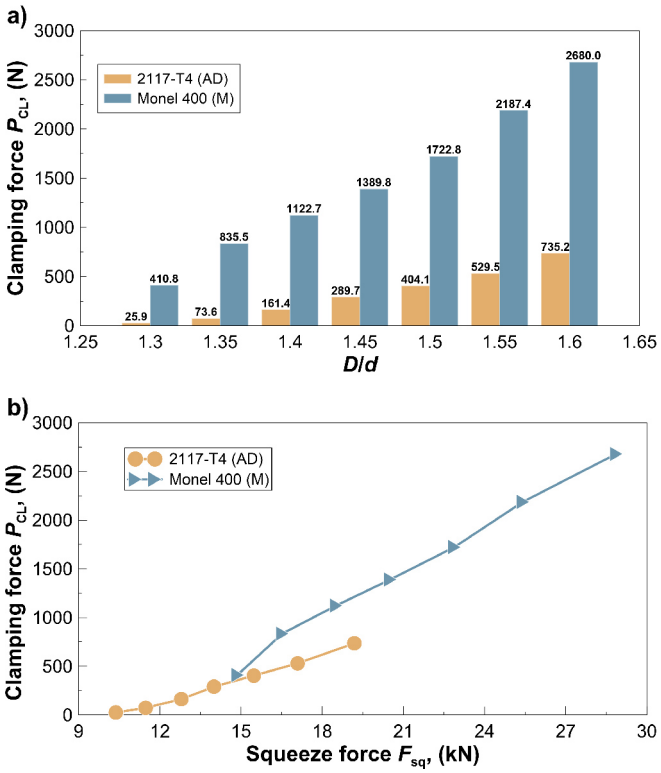

Fig. 21. P_{CL} force for 2024-T3 sheets connected with MS20470AD5-5 or MS20615-5M5 rivets as a function of: (a) D/d ratio; (b) F_{sq} force

and the P_{CL} force shows that the clamping force remaining in the joint after the riveting process is significantly lower than the F_{sq} force (Fig. 21b). For considered joint thicknesses and D/d ratios (1.3÷1.6), the P_{CL} force is approximately 0.16%÷3.85% and 2.75%÷9.44% of the F_{sq} force for rivets made of A2117-T4 and Monel 400, respectively. Additionally, Fig. 22 shows that after the riveting process (before joint loading), the P_{CL} force value for both rivet materials is almost the same in each rivet row, which means that its value does not depend on the row of rivet from which it is determined.

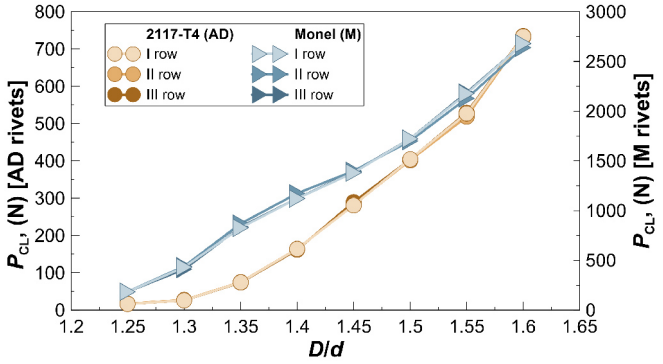

Fig. 22. Comparison of the P_{CL} force in three different rivet rows for joints with MS20470AD5-5 or MS20615-5M5 rivets

The most important observation resulting from FEA is that during joint loading, through the higher P_{CL} force, the friction force (T_{FR}) in joints with a higher D/d ratio will be higher than in the case of joints with a small D/d ratio, which will also affect the fretting phenomenon in these joints [8]. Similarly, for the same D/d ratio, the contribution of the T_{FR} force to total load transfer (T_{TR}) in joints with M rivets will be greater than in joints with AD rivets. An increase in the contribution of the T_{FR} force to the total T_{TR} force transmitted by a given rivet suggests that the bearing pressure exerted by the rivet shank on the rivet hole should be lower. However, a precise determination of the contribution of T_{FR} to load transfer requires further FE analyses for the investigated riveted lap joints with various levels of applied load, which will be the subject of further research.

7. CONCLUSIONS

The experimental and numerical results presented in this paper lead to the following conclusions:

The performed static compression tests revealed that the material of rivets made of nickel-copper alloy (Monel 400) is a material with significantly higher mechanical properties compared to the material of rivets made of aluminium alloy (2117-T4). Monel 400 has both Young's modulus (173 GPa) and yield strength (438 MPa) twice as high as AA2117-T4 (Young's modulus 70 GPa and yield strength 221 MPa).

The experimental investigation showed that within a very wide range of rivet squeezing degrees (D/d = 1.25÷1.6), MS20615-5M5 (Monel 400) rivets require 42% to 55% higher squeeze forces to obtain the same diameter and height of the driven rivet head than MS20470AD5-5 (AA2117-T4) rivets, despite the same initial rivet diameter and length.

The measurements indicated that the rivet hole expansion is significantly larger in the sheet on the driven head side than on the manufactured head side, and at the same time, the hole expansion increases with the squeeze force level. For the considered D/d ratios (1.3, 1.5, and 1.6) the hole expansion for rivets made of Monel 400 at a given D/d ratio is significantly larger (at least twice) than for rivets made of AA2117-T4. This is because the sheet material (AA2024-T3) exhibits less resistance during the expansion of the rivet shank made of a harder alloy (Monel 400) than of a softer alloy (AA2117-T4).

The results from the FE models showed that regardless of the rivet material and the D/d ratio, the residual radial stresses are negative (compressive) and non-uniformly distributed in the joint thickness direction and agree qualitatively with the hole expansion distribution. With the same driven rivet head dimensions, radial stresses in joints with rivets made of Monel 400 are higher (18%÷43%) than in joints with rivets made of AA2117-T4. This is due to the higher mechanical properties of MS20615-5M5 rivets than MS20470AD5-5 rivets.

The FE analyses indicated that for both considered rivet materials the distribution and nature of residual hoop stresses strongly depend on the D/d degree. For less squeezed rivets (D/d = 1.25÷1.3), positive (tensile) stresses most often occur in the vicinity of the rivet hole, while for more severely squeezed rivets (D/d = 1.4 and above), positive stresses are shifted to a certain distance from the rivet hole and negative (compressive) stresses appear in its close vicinity. The same D/d ratio causes significantly greater compressive hoop stresses in joints with rivets made of Monel 400, both in value and range, than those observed in joints with rivets made of AA2117-T4. This suggests that the MS20615-5M5 rivets result in a larger plastic deformation zone of the sheets around the rivet hole compared to the MS20470AD5-5 rivets. The compressive hoop stresses around the rivet hole partially explain the increased fatigue life and the changed crack initiation location in riveted joints with higher squeeze force.

Regardless of the rivet material, the highest clamping stresses occur at the rivet hole edge and decrease rapidly with distance from this location. Simultaneously, the value and range of these stresses significantly increase with the squeeze force level. Considering the same driven rivet head dimensions, the clamping stress values observed in joints with Monel 400 rivets are several times higher than in joints with AA2117-T4 rivets. A higher value and a larger annular clamping stress zone cause greater stiffening of the joined sheets beneath the rivet heads, which will affect the secondary bending phenomenon and the crack path location.

FE analyses revealed that the clamping force value systematically increases with increasing squeeze force. For the considered D/d ratios (1.3÷1.6) it constitutes 0.16%÷3.85% and 2.75%÷9.44% of the total squeeze force for the AA2117-T4 and Monel 400 rivets, respectively. Moreover, for the same D/d ratio, the clamping force reaches values 3.6÷15.9 times higher in joints with Monel 400 rivets than in joints with AA2117-

T4 rivets. This indicates that due to the higher clamping force at the same D/d ratio, the contribution of friction force in the total force transmitted by a given row of rivets in joints with MS20615-5M5 rivets will be higher than in joints with MS20470AD5-5 rivets, which will also affect the fretting phenomenon in these joints during their cyclic loading.

ACKNOWLEDGEMENTS

This work was funded by the AGH University of Science and Technology, Faculty of Mechanical Engineering and Robotics [grant No. 16.16.130.942]. The funders had no role in study design, data collection and analysis, decision to publish, or preparation of the manuscript.

The article was co-financed from the state budget of Poland and awarded by the Minister of Science within the framework of the Excellent Science II Programme.

REFERENCES

[1] H. Zhao *et al.*, "A review on solid riveting techniques in aircraft assembling," *Manuf. Rev.*, vol. 7, p. 40, 2020, doi: 10.1051/mfreview/2020036.

[2] M. Skorupa and A. Korbel, "Modelling the secondary bending in riveted joints with eccentricities," *Arch. Mech. Eng.*, vol. 55, no. 4, pp. 369–387, 2008, doi: 10.24425/ame.2008.131633.

[3] Y. Yang, Y. Bao, X. Liu, J. Wang, and F. Du, "Progressive failure analysis of Composite/Aluminum riveted joints subjected to Pull-Through loading," *Chin. J. Mech. Eng.*, vol. 36, no. 1, p. 10, 2023, doi: 10.1186/s10033-023-00839-z.

[4] L. Zhang, W. Chen, Z. Wang, and X. Wang, "Effect of ultrasonic amplitude and riveting speed on mechanical properties of Ti-45Nb riveted lap joints," *Eng. Fail. Anal.*, vol. 163, p. 108515, 2024, doi: 10.1016/j.engfailanal.2024.108515.

[5] M.C.Y. Niu, *Airframe stress analysis and sizing*. Hong Kong: Conmilit Press Ltd., 1999.

[6] A. Skorupa and M. Skorupa, *Riveted lap joints in aircraft fuselage*. Dordrecht, Heidelberg, New York, London: Springer, 2012.

[7] A. Kubit, Ł. Święch, T. Trzepieciński, and K. Faes, "Experimental Analysis of the Post-Buckling Behaviour of Compressed Stiffened Panel with Refill Friction Stir Spot Welded and Riveted Stringers," *Adv. Sci. Technol.–Res. J.*, vol. 16, no. 2, pp. 159–167, 2022, doi: 10.12913/22998624/146899.

[8] A. Korbel, "Effect of aircraft rivet installation process and production variables on residual stress, clamping force and fatigue behaviour of thin sheet riveted lap joints," *Thin-Walled Struct.*, vol. 181, p. 110041, 2022, doi: 10.1016/j.tws.2022.110041.

[9] National Transportation Safety Board, "Aloha Airlines, Flight 243, Boeing 737–200, N73711, Near Maui, Hawaii, April 28, 1988," Washington, DC, USA, Rep. NTSB/AAR-89/03, 1989.

[10] National Transportation Safety Board, "Aviation Investigation Final Report, Accident Bell UH-1H N97NW, Monday 12 August 1996," USA, Rep. NTSB/SEA96FA187.

[11] National Transportation Safety Board, "Aviation Investigation Final Report, Accident Garlick TH-1L (Bell 204) N465JR, Tuesday 5 November 1996," USA, Rep. NTSB/SEA97LA025.

[12] J. Schijve, "Multiple-site damage in aircraft fuselage structures," *Fatigue Fract. Eng. Mater. Struct.*, vol. 18, no. 3, pp. 329–344, 1995, doi: 10.1111/j.1460-2695.1995.tb00879.x.

[13] J.J. Homan and A.A. Jongebreur, "Calculation method for predicting the fatigue life of riveted lap joints," in *ICAF 1993, Durability and Structural Integrity of Airframes*, A.F. Blom, Ed. Stockholm, Sweden: EMAS, 1993, pp. 175–190.

[14] G.K. Das, M. Miller, T. Sovar, "Durability assessment of fuselage single shear lap joint with pads," in *ICAF 2001, Design for Durability in The Digital Age*, J. Rouchon, Ed. Tolouse, France: Cepadues Edition, 2001, pp. 567–595.

[15] J. Schijve, *Fatigue of structures and materials*. 2nd ed. Dordrecht, Heidelberg, New York, London: Springer, 2009.

[16] H. Yu, B. Zheng, X. Xu, and X. Lai, "Residual stress and fatigue behavior of riveted lap joints with various riveting sequences, rivet patterns, and pitches," *Proc. Inst. Mech. Eng. Part B-J. Eng. Manuf.*, vol. 233, no. 12, pp. 2306–2319, 2019, doi: 10.1177/0954405419834481.

[17] M. Skorupa, T. Machniewicz, A. Skorupa, J. Schijve, and A. Korbel, "Fatigue life prediction model for riveted lap joints," *Eng. Fail. Anal.*, vol. 53, pp. 111–123, 2015, doi: 10.1016/j.engfailanal.2015.03.013.

[18] M. Skorupa, T. Machniewicz, A. Skorupa, and A. Korbel, "Fatigue life predictions for riveted lap joints," *Int. J. Fatigue*, vol. 94, pp. 41–57, 2017, doi: 10.1016/j.ijfatigue.2016.09.007.

[19] K. Ding, Y. Yang, Z. Wang, T. Zhang, and W. Guo, "Relationship between local strain energy density and fatigue life of riveted Al-Li alloy plate," *Theor. Appl.Fract. Mech.*, vol. 125, p. 103672, 2023, doi: 10.1016/j.tafmec.2022.103672.

[20] C.D. Rans, R.C. Alderliesten, and P.V. Straznicky, "Assessing the effects of riveting induced residual stresses on fatigue crack behaviour in lap joints by means of fractography," *Int. J. Fatigue*, vol. 31, no. 2, pp. 300–308, 2008, doi: 10.1016/j.ijfatigue.2008.08.005.

[21] A. Skorupa, M. Skorupa, T. Machniewicz, and A. Korbel, "An experimental investigation on crack initiation and growth in aircraft fuselage riveted lap joints," *Mater. Sci. Forum*, vol. 726, pp. 211–217, 2012, doi: 10.4028/www.scientific.net/msf.726.211.

[22] J. Zou, Z. Yuechao, and Z. Feng, "Multiple crack growth simulation for lap-joints based on three-dimensional finite element analysis," *Aircr. Eng. Aerosp. Technol.*, vol. 94, no. 10, pp. 1834–1844, 2022, doi: 10.1108/aeat-01-2021-0026.

[23] F. Zakar, "Multiple-site fatigue cracking of fuselage structure due to improper rivet installation," *J. Fail. Anal. Prev.*, vol. 24, no. 1, pp. 24–31, 2023, doi: 10.1007/s11668-023-01801-w.

[24] Y. Liao *et al.*, "Effect of rivet arrangement on fatigue performance of electromagnetic riveted joint with Φ10 mm diameter rivet," *Int. J. Fatigue*, vol. 176, p. 107892, 2023, doi: 10.1016/j.ijfatigue.2023.107892.

[25] M. Zhang, Z. Cao, Y. Guo, Y. Cao, G. Zheng, and L. Huo, "Stress, damage, and fatigue performance analysis of CFRP/Al double-sided countersunk riveted joints with variable rivet-hole clearance," *Int. J. Fatigue*, vol. 186, p. 108385, 2024, doi: 10.1016/j.ijfatigue.2024.108385.

[26] M. Skorupa, T. Machniewicz, A. Skorupa, and A. Korbel, "Effect of load transfer by friction on the fatigue behaviour of riveted lap joints," *Int. J. Fatigue*, vol. 90, pp. 1–11, 2016, doi: 10.1016/j.ijfatigue.2016.04.005.

[27] C. Zeng, J.T. Xue, X.Y. Liu, and W. Tian, "Design variables influencing the fatigue of Al 2024-T3 in riveted aircraft lap joints: Squeeze force and initial fit tolerance," *Int. J. Fatigue*, vol. 140, p. 105751, 2020, doi: 10.1016/j.ijfatigue.2020.105751.

[28] R.P.G. Müller, "An experimental and analytical investigation on the fatigue behaviour of fuselage riveted lap joints." PhD thesis, Delft University of Technology, The Netherlands, 1995.

[29] M. Skorupa, A. Skorupa, T. Machniewicz, and A. Korbel, "An experimental investigation on the fatigue performance of riveted lap joints," in *ICAF 2009, Bridging the Gap Between Theory and Operational Practice*, M.J. Boss, Ed. Dordrecht, Heidelberg, New York, London: Springer, 2009, pp. 449–473, doi: 10.1007/978-90-481-2746-7_26.

[30] J. Papuga and J. Stejskal, "Effect of some riveting process parameters on the fatigue life of double-shear lap joints," *Eng. Fail. Anal.*, vol. 134, p. 106008, 2021, doi: 10.1016/j.engfailanal.2021.106008.

[31] A. Skorupa, M. Skorupa, T. Machniewicz, and A. Korbel, "Fatigue crack location and fatigue life for riveted lap joints in aircraft fuselage," *Int. J. Fatigue*, vol. 58, pp. 209–217, 2014, doi: 10.1016/j.ijfatigue.2013.01.014.

[32] A. Brown and P. Straznicky, "Simulating fretting contact in single lap splices," *Int. J. Fatigue*, vol. 31, no. 2, pp. 375–384, 2008, doi: 10.1016/j.ijfatigue.2008.07.012.

[33] J.K. Martinez, P.B. Keating, P. Montenegro, and J.A.F.O. Correia, "Fracture mechanics analysis of the effect of clamping stress on the fatigue life of riveted built-up railroad girders under variable amplitude loading," *Eng. Fail. Anal.*, vol. 118, p. 104812, 2020, doi: 10.1016/j.engfailanal.2020.104812.

[34] C. Rans, P.V. Straznicky, and R. Alderliesten, "Riveting process induced residual stresses around solid rivets in mechanical joints," *J. Aircr.*, vol. 44, no. 1, pp. 323–329, 2007, doi: 10.2514/1.23684.

[35] M. Li, W. Tian, J. Hu, C. Wang, Z. Shi, and W. Liao, "Influence of riveting die configuration and squeeze force on the mechanical properties and fatigue behavior of aircraft lap joints," *Eng. Fail. Anal.*, vol. 142, p. 106772, 2022, doi: 10.1016/j.engfailanal.2022.106772.

[36] J. Liu, A. Zhao, Z. Ke, Z. Zhu, and Y. Bi, "Influence of rivet diameter and pitch on the fatigue performance of riveted lap joints based on stress distribution analysis," *Materials*, vol. 13, no. 16, p. 3625, 2020, doi: 10.3390/ma13163625.

[37] X. Zhang *et al.*, "Effect of punch type on microstructure and mechanical properties of aluminum alloy structures prepared by electromagnetic riveting," *Arch. Civ. Mech. Eng.*, vol. 24, no. 3, 2024, doi: 10.1007/s43452-024-00985-8.

[38] D. Leonetti, J. Maljaars, G. Pasquarelli, and G. Brando, "Rivet clamping force of as-built hot-riveted connections in steel bridges," *J. Construct. Steel Res.*, vol. 167, p. 105955, 2020, doi: 10.1016/j.jcsr.2020.105955.

[39] C. Rans, P. Straznicky, and R. Alderliesten, "Effects of rivet installation on residual stresses and secondary bending stresses in a riveted lap joint," *54th AIAA/ASME/ASCE/AHS/ASC Structures, Structural Dynamics, and Materials Conference*, 2007, doi: 10.2514/6.2007-2307.

[40] O.K. Bedair and G.F. Eastaugh, "A numerical model for analysis of riveted splice joints accounting for secondary bending and plates/rivet interaction," *Thin-Walled Struct.*, vol. 45, no. 3, pp. 251–258, 2007, doi: 10.1016/j.tws.2007.03.001.

[41] T. Machniewicz, A. Korbel, M. Skorupa, and J. Winter, "Analytical, numerical and experimental investigation of the secondary bending of riveted lap joints," *AIP Conf. Proc.*, vol. 2028, p. 020010, 2018, doi: 10.1063/1.5066400.

[42] G. Li, G. Shi, and N.C. Bellinger, "Studies of residual stress in Single-Row Countersunk Riveted lap joints," *J. Aircr.*, vol. 43, no. 3, pp. 592–599, 2006, doi: 10.2514/1.18128.

[43] C. Zeng, W. Tian, X.Y. Liu, and J.T. Xue, "Experimental and numerical studies of stress/strain characteristics in riveted aircraft lap joints," *J. Mec. Sci. Technol.*, vol. 33, no. 7, pp. 3245–3255, 2019, doi: 10.1007/s12206-019-0620-7.

[44] Y. Kang, H. Xiao, Z. Wang, G. Li, and Y. Chen, "Three-Dimensional characterization of residual stress in aircraft riveted panel structures," *Aerospace*, vol. 11, no. 7, p. 552, 2024, doi: 10.3390/aerospace11070552.

[45] M. Skorupa, T. Machniewicz, A. Skorupa, and A. Korbel, "Investigation of load transmission throughout a riveted lap joint," *Procedia Eng.*, vol. 114, pp. 361–368, 2015, doi: 10.1016/j.proeng.2015.08.080.

[46] H. Huan and M. Liu, "Effects of squeeze force on static behavior of riveted lap joints," *Adv. Mech. Eng.*, vol. 9, no. 5, 2017, doi: 10.1177/1687814016686891.

[47] C. Lei, Q. Huang, and Y. Bi, "Tensile load distribution improvement of Three-Row riveted lap joint based on different squeezing displacement combinations," *Coatings*, vol. 11, no. 7, p. 856, 2021, doi: 10.3390/coatings11070856.

[48] Z. Silvayeh, M. Brillinger, and J. Domitner, "Deformation behavior of aluminum alloy rivets for aerospace applications," *J. Mater. Res. Technol.*, vol. 33, pp. 3482–3491, 2024, doi: 10.1016/ j.jmrt.2024.09.259.

[49] J. Aegerter, H.-J. Kühn, H. Frenz, and C. Weißmüller, "EN ISO 6892-1:2009 Tensile Testing: Initial Experience from the Practical Implementation of the New Standard," *Mater. Test.*, vol. 53, no. 10, pp. 595–603, 2011, doi: 10.3139/120.110269.

[50] M. Skorupa, T. Machniewicz, A. Skorupa, and A. Korbel, "Fatigue strength reduction factors at rivet holes for aircraft fuselage lap joints," *Int. J. Fatigue*, vol. 80, pp. 417–425, 2015, doi: 10.1016/j.ijfatigue.2015.06.025.

[51] Standard Test Methods of Compression Testing of Metallic Materials at Room Temperature, ASTM E9.

[52] Metallic materials – Tensile testing – Part 1: Method of test at ambient temperature, PN-EN 10002-1:2004.

[53] Dantec Dynamics. *ISTRA 4D. Software Manual Q-400 System. Manual Version 4.4.6*, vol. 2, 2017.

[54] G. Li, G. Shi, and N.C. Bellinger, "Assessing the riveting process and the quality of riveted joints in aerospace and other applications," in *Elsevier eBooks*, 2012, pp. 181–214. doi: 10.1533/9780857095169.2.179.

[55] S. Pourhassan, P.J. Tavares, and P.M.G.P. Moreira, "Material properties of 2024-T3 ALCLAD and 2124-T851 aluminum alloys using 2D and 3D Digital Image Correlation techniques," *Procedia Struct. Integr.*, vol. 5, pp. 1355–1362, 2017, doi: 10.1016/j.prostr.2017.07.198.

[56] *Metallic materials and elements for aerospace vehicle structures*, Military handbook, 1998.

[57] *Rivet, solid, universal head, aluminum alloy and titanium columbium alloy*, NASM20470.

[58] *Rivet, solid, universal head, brass, copper, nickel-copper alloy*, NASM20615.

[59] Boeing Service Bulletin, *Body skin lap joint inspection and repair*. 737-53-1039, 1972.

[60] H.J. Hoever ten, L. Schra, A.L.P.J. Michielsen, H. Vlieger, "*Residual Strength of Stiffened Panels with Multiple Site Damage*," DOT/FAA, Washington, DC, DOT/FAA/AR-98/53, 1999.

[61] Ansys Inc, ANSYS Mechanical User's Guide: Release 21.2, Ansys Inc. Canonsburg, PA, 2020.

[62] G. Li, G. Shi, and N. Bellinger, "Effects of fastener clearance fit and friction coefficient on the stress condition in triple-row riveted lap joints," in *Proc. 51st AIAA/ASME/ASCE/AHS/ASC Structures, Structural Dynamics and Materials Conference*, Orlando, USA, AIAA Paper, 2010, pp. 1–24.

[63] A. Kondo, T. Kasahara, and A. Kanda, "A Simplified Finite Element Model of Riveted Joints for Structural Analyses with Consideration of Nonlinear Load-Transfer Characteristics," *Aerospace*, vol. 8, no. 7, p. 196, Jul. 2021, doi: 10.3390/aerospace8070196.

[64] M. Li, W. Tian, J. Hu, C. Wang, and W. Liao, "Study on shear behavior of riveted lap joints of aircraft fuselage with different hole diameters and squeeze forces," *Eng. Fail. Anal.*, vol. 127, p. 105499, May 2021, doi: 10.1016/j.engfailanal.2021.105499.

[65] Ansys Inc, ANSYS Mechanical Structural Nonlinearities, in: Lecture 3: Introduction to contact: Release, vol. 13, Ansys Inc., 2010.

[66] X. Chen and Y. Liu, *Finite Element Modeling and Simulation with ANSYS Workbench*. Boca Raton, London, New York: CRC Press, Taylor & Francis Group, 2015.

[67] Ansys Inc, ANSYS Mechanical, Introduction to ANSYS Meshing, in: Lecture 4: Meshing Techniques: Release, vol. 16, Ansys Inc., 2015.

[68] M. Skorupa, A. Korbel, A. Skorupa, and T. Machniewicz, "Observations and analyses of secondary bending for riveted lap joints," *Int. J. Fatigue*, vol. 72, pp. 1–10, 2014, doi: 10.1016/j.ijfatigue.2014.10.008.

[69] M. Skorupa, T. Machniewicz, A. Korbel, and A. Skorupa, "Rivet flexibility and load transmission for a riveted lap joint," *Arch. Mech. Eng.*, vol. 57, no. 3, pp. 235–245, 2010, doi: 10.2478/v10180-010-0012-0.

[70] J. Hu, J. Jin, S. Xuan, S. Mi, W. Tian, and W. Liao, "Influence of cyclical hygrothermal aging on mechanical response and structural durability of composite bolted interference-fit joints," *Thin-Walled Struct.*, vol. 173, p. 108997, 2022, doi: 10.1016/j.tws.2022.108997.

[71] L. Zhao, X. He, B. Xing, X. Zhang, C. Deng, and Y. Liu, "Fracture mechanism of titanium sheet self-piercing riveted joints," *Thin-Walled Struct.*, vol. 144, p. 106353, 2019, doi: 10.1016/j.tws.2019.106353.